JPE 19-2-9

https://doi.org/10.6113/JPE.2019.19.2.431
ISSN(Print): 1598-2092 / ISSN(Online): 2093-4718

DAB Converter Based on Unified High-Frequency Bipolar Buck-Boost Theory for Low Current Stress

Jia-rong Kan†, Yao-dong Yang*, Yu Tang**, Dong-chun Wu*, Yun-ya Wu*, and Jiang Wu***

†,*Department of Electrical Engineering, Yancheng Institute of Technology, Yancheng, China
**Department of Electrical Engineering, Hebei University of Technology, Tianjin, China
***Suzhou Power Supply Company, National Grid Jiangsu Electric Power Co., Suzhou, China

Abstract

This paper proposes a unified high-frequency bipolar buck-boost (UHFBB) control strategy for a dual-active-bridge (DAB), which is derived from the classical buck and boost DC/DC converter. It can achieve optimized current stress of the switches and soft switching in wider range. The UHFBB control strategy includes multi-control-variables, which can be achieved according to an algorithm derived from an accurate mathematical model. The design method for the parameters, such as the transformer turns ratio and the inductance, are shown. The current stress of the switches is analyzed for selecting an optimal inductor. The analysis is verified by the experimental results within a 500W prototype.

Key words: BCM, Current stress, DAB, DCM, High-frequency bipolar buck-boost, Multi-parameters solving

I. INTRODUCTION

Bidirectional DC/DC converters (BDCs) are widely used in aerospace applications [1], electrical vehicle chargers [2], distributed generation (DG) systems and AC or DC micro-grids [3] due to their bidirectional power flow, low cost, small volume and low weight. Therefore, they have attracted a lot of attention.

BDCs can be divided into two class, non-isolated and isolated [4], [5]. The non-isolated BDC is hard to achieve a high conversion efficiency if a high step-up or step-down voltage ratio is necessary. Meanwhile, the isolated BDC can match the input and output voltage by using a high frequency transformer and it can easily obtain a high efficiency. Generally, BDCs include current-fed and voltage-fed converters [6], [7]. In the current-fed BDC, the spike voltage is usually across the switches and a clamped circuit should be included in the converter, which increases the complexity and cost of the converter. The switches in the voltage-fed BDC are all clamped by filter capacitors. The advantages of the voltage-fed BDC have led to its wide adoption. The voltage-fed BDC can be achieved by reorganizing the classical DC/DC converter. The reorganized BDCs are symmetrical about the transformer, and include the flyback BDC [8], the flyback-forward hybrid BDC [9], the half-bridge BDC [10], the full-bridge BDC [11], etc. In large or medium power applications, the dual-active-bridge (DAB) is usually adopted due to its zero-voltage switching (ZVS) and its bidirectional power flow by a simple phase-shift control strategy [7]. In the DAB, the phase and pulse width of the AC square-wave voltages on both sides of the transformer can all be adjusted to achieve optimal efficiency [12], [13]. In recent years, many research results have been achieved in an effort to decrease the circulating energy, the current stress of the switches and the total loss [14].

The authors of [15] proposed a definition of extended phase shift to decrease the circulating energy and the switches conduction loss, which achieved a high efficiency. However, there are three independent control variables, which are the primary-side full-bridge duty ratio D1, the secondary-side full-bridge duty ratio D2 and their phase shift angle ϕ. The most optimized of the three variables method is not proposed in the paper and the circulating energy is not at the minimum value

Manuscript received Jul. 14, 2018; accepted Nov. 10, 2018
Recommended for publication by Associate Editor Jongwon Shin.
†Corresponding Author: kanjr@163.com
Tel: +86-515-88168194, Fax: +86-515-88168666, Yancheng Institute of Technology
*Dept. of Electrical Eng., Yancheng Institute of Technology, China
**Dept. of Electrical Eng., Hebei University of Technology, China
***Suzhou power supply company, National grid Jiangsu Electric Power Co., China

because D1 is a fixed value in the control strategy. A double phase-shift control strategy is proposed in an effort to achieve the minimum peak current [16]. However, D1 = D2 is designed for convenient control. Therefore, this method can be further optimized. According to the output power, a segment variable-frequency strategy is proposed to guarantee the optimized efficiency [17]. On the one hand, the realization of the segment variable-frequency is difficult to achieve. On the other hand, the adopted triangle current control results in more current stress. The full power loss model is built and the three variables mentioned above, D1, D2 and ϕ, are determined according to the principle of the minimum power loss [18]. However, the operation condition depends on the accuracy of the loss model and the modeling process is complicated. Moreover, ZVS in the DAB is somewhat determined by the workload [12].

The conventional control strategy for a DAB comprises of a voltage outer-loop and a current inner-loop [19], [20]. The feedback variable of the current inner-loop is the inductor current, which is generally filtered to obtain a smooth variable. The added low-pass filter affects the dynamic performance of the DAB. Hence, predictive current control is widely investigated [21]. However, the control effect of the predictive current control is determined by the accuracy of the measurement.

This paper proposes a method based on the unified high-frequency bipolar buck-boost theory for the DAB to overcome the shortcomings mentioned in [22]. The inductor current is designed in the discontinuous conduction mode (DCM) or the boundary conduction mode (BCM) in half of a switching cycle and the switching frequency is fixed, which guarantees that the switches realize ZVS or ZCS. Moreover, an algorithm for solving multi-variables is proposed for optimizing the current stress. The current sensor is removed and the dynamic performance is enhanced. Experimental results verify the high performance of the proposed method.

II. Motivation for Introducing the Unified Bipolar Buck-Boost Theory into a DAB

Fig. 1 shows the topology of a DAB which comprises of a low-voltage-side (LVS) full-bridge formed by S1-S4, a high-voltage-side (HVS) full-bridge formed by S5-S8, an inductor L, and a high-frequency transformer T with a turns ratio of 1:n. C_{r1}-C_{r8} and D1-D8 are the parasitic capacitors and body diodes of the switches S1-S8, respectively. U_{in} and U_o are the input and output voltages, respectively. C_1 and C_2 are the filter capacitors in the LVS and HVS. respectively. i_L is the current through the buffering inductor L. i_S and u_S are the secondary-side current and voltage of the transformer, respectively. u_{L1} and u_{L2} are the input-terminal and output-terminal voltages of the buffering inductor, respectively. I_o is the output current of the DAB, and u_{L2} is input voltage of the transformer T.

In the existing control strategy for the DAB, some shortcomings, such as switching surges, circulating current and high current stress of the switches, overly complicated control strategy, etc., decrease the efficiency and block the widespread use of the DAB. These shortcomings are expected to be overcome after using the method proposed in this paper.

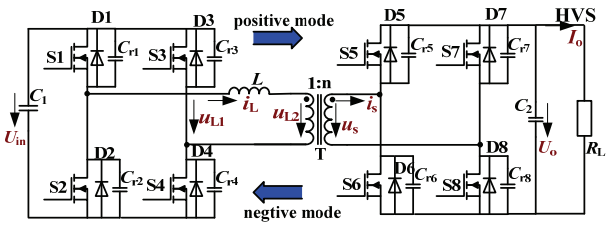

Fig. 1. Topology of a DAB.

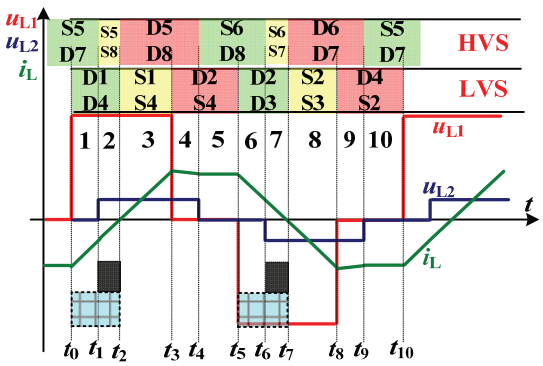

Fig. 2. Operational waveforms of a DAB controlled by the dual-phase-shift control strategy.

A. Hard Switching

Under most conditions, the switches can achieve ZVS in the existing control strategy. However, there are some special conditions. The reason for the high diode reverse recovery loss under a light load with the conventional single phase-shift control strategy is analyzed in [23]. Moreover, there is also switching loss in some of the improved control strategies [15], [16], [23]. Fig. 2 shows an example of a DAB controlled by the dual-phase-shift strategy [16].

There are 10 modes in a switching cycle in Fig. 2. There is no surge voltage across the switches in the LVS because i_L lags behind u_{L1}. However, a surge voltage occurs repeatedly in the HVS switches in the transition from mode 1 (6) to mode 2 (7). The diode D7 and the switch S5 are conducting in state 1. Then the switch S7 is turned off and S8 is turned on when the state changes from mode 1 to mode 2. At this time, the diode D7 is immediately switched from a forward bias condition to a reverse bias condition, and the switch S7 is turned off with a large reverse recovery loss. Therefore, there is high switching loss condition as shown in Fig. 2. The cyan and black boxes shown in Fig. 2 show that there is circulating energy to the full-bridge in the LVS and HVS in the corresponding intervals because of the opposite polarities of the voltage and current.

B. Circulating Current and High Current Stress

Many methods have been proposed to decrease or eliminate

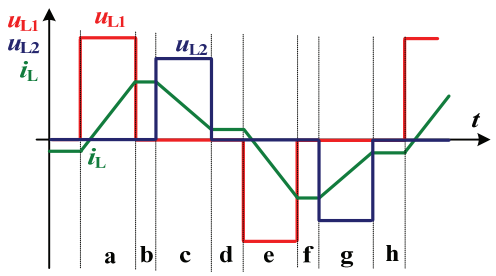

Fig. 3. Waveforms of the control strategy in [14].

circulating current [14], [15]. Moreover, a lot of studies have tried to achieve the minimum RMS value or peak value of i_L. These two objections should be concurrent, which means that the RMS value of i_L is decreased if the circulating current is well restrained [16], [24]. However, the existing control strategies cannot a good match for these two objectives. For example, main waveforms of the control strategy in [14] are shown in Fig. 3. It completely eliminates the circulating current. However, the RMS value of i_L is still high. The duty ratios of the two bridges in both sides of the transformer are designed too short. Then the zero-time intervals of u_{L1} and u_{L2} are very long. There is current flowing though the switches in these time intervals. In half a switching cycle, the current in modes b-d cannot produce active power to the bridge in the LVS and the current in modes a, b and d cannot produce active power to the bridge in the HVS.

C. Complexity of Control Strategy

In order to achieve a high efficiency, some control strategies adopt composite modulation methods according to the power boundary [24]-[27]. Although the composite modulation methods can obtain an optimized switching current stress, the calculation process is very complicated and it requires a high-performance digital chip to perform the calculations. On the other hand, the power boundary may have no closed-form solution and a numerical solver has to be used to determine the boundary power [24].

Therefore, the objective of this paper is to propose a simple modulation so the DAB can achieve soft switching, no circulating current, low current stress and high efficiency.

III. Principle of High-Frequency Bipolar Buck-Boost Theory

There is a large circulating current when using the conventional phase-shift strategy. If the stored energy in the buffering inductor L is entirely released in a positive or negative half switching cycle, that is the current i_L=0 at the beginning of a positive or negative half switching cycle, the problem of circulating current can be solved.

A reasonable turns ratio of the transformer 'n' can match the unbalance between the input and output voltages. However, the fluctuation of U_{in} and U_o is very large and the amplitude

TABLE I
Switch State of a DC Converter

	Buck			Boost		
A	1	0	0	1	1	0
B	1	1	0	0	1	0

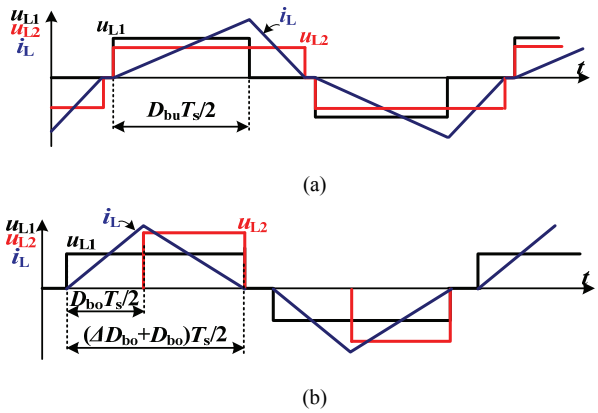

Fig. 4. Modulation strategy for a high-frequency bipolar buck-boost voltage. (a) High-frequency bipolar buck operation waveform (U_{in}>U_o/n). (b) High-frequency bipolar boost operation waveform (U_{in}<U_o/n).

relationship between u_{L1} and u_{L2} is not fixed. Therefore, the operation principle of a conventional buck and boost DC/DC converter can be introduced into DABs when they are operated in the DCM or the BCM. Assuming the input and output voltages of a buck and boost DC/DC converter are also U_{in} and U_o, the voltage across the inductor can be expressed as:

$$u_L = AU_{in} - BU_o \tag{1}$$

Where A and B are the states on the two sides of the inductor in a buck or boost converter, and their values are shown in Table I. There are three modes in a switching cycle. The three modes are the current-increasing stage, the current-decreasing stage and the zero-current stage. If this operation principle is expanded to a high-frequency bipolar topology, the waveforms of u_{L1}, u_{L2} and i_L are shown in Fig. 4, which form the high-frequency bipolar buck or boost operation principle. Where, D_{bu} and D_{bo} are the bipolar buck and boost duty ratios, respectively.

Setting a voltage as threshold value, a proper operation mode can be selected according to the value of U_{in} and U_o, which can guarantee ZVS or ZCS of all the switches. However, this method has a number of obvious shortcomings.

1) When compared with the continuous conduction mode, the peak value of i_L is larger in this method, which results in a larger current stress and a lower efficiency.
2) The converter may be unstable at the time of the transition from the buck mode to the boost mode, and vice versa. Moreover, the converter cannot work when U_{in}=U_o/n.

In order to retain the characteristic of ZVS and ZCS and to

TABLE II
UNIFIED HIGH-FREQUENCY BIPOLAR BUCK/BOOST CONTROL STRATEGY

Duty ratio	Positive half cycle				Negative half cycle			
	d_1	d_2	d_3	d_4	d_1	d_2	d_3	d_4
A	1	1	0	0	-1	-1	0	0
B	0	1	1	0	0	-1	-1	0

decrease the current stress of the switches, i_L should be operated in the DCM or the BCM in every half switching cycle. Therefore, a unified high-frequency bipolar buck-boost control strategy can also be explored. Setting the voltage across the inductor is still satisfied with (1). This paper proposed the method shown in Table II.

A switching cycle is divided into a positive and negative half cycle. Each half cycle has four modes and their duty ratios are d_1, d_2, d_3 and d_4, respectively. Their relationships are shown in Fig. 5.

$$\begin{cases} d_1 = \dfrac{\text{duration time of (A=1\&B=0)}}{0.5T_S} \\ d_2 = \dfrac{\text{duration time of (A=1\&B=1)}}{0.5T_S} \\ d_3 = \dfrac{\text{duration time of (A=0\&B=1)}}{0.5T_S} \\ d_4 = \dfrac{\text{duration time of (A=0\&B=0)}}{0.5T_S} \end{cases} \text{positive half cycle} \quad (2)$$

In a positive half cycle, the operation principle of the former two modes whose duty ratios are d_1 and d_2 is similar to a boost DC/DC converter, and the operation principle of the medium two modes whose duty ratios are d_2 and d_3 is similar to a buck DC/DC converter. That is, the proposed control strategy in Table II is essentially a hybrid control combined with the buck and boost operation principle. The function of increasing or decreasing the voltage can be easily realized if the multi-duty-ratios are adjusted. Moreover, the control variables vary continuous. According to the input and output voltage values, not all of the four modes are included in a half switching cycle.

When $nU_{in}<U_o$, the converter can be viewed as operating in the boost mode, and Fig. 5 shows the three different conditions. The inductor current i_L is running in the DCM in a half switching cycle and there is no the third mode under a light load, that is $d_3=0$, as shown in Fig. 5(a). The converter operating mode is shift from the DCM to the boundary-BCM (B-BCM) when the output power is equal to the boundary power P_{B_boost}. In the B-BCM, d_3 and d_4 are always equal to zero. The corresponding waveforms are shown in Fig. 5(b). With the power further increasing, the converter is operated in the BCM and $d_3>0$. The waveforms shown in Fig. 5(c) show that part buck operating mode joins in the modulation strategy to guarantee the BCM.

When $nU_{in}>U_o$, the converter can be viewed as operating in the buck mode. The corresponding waveforms are shown in

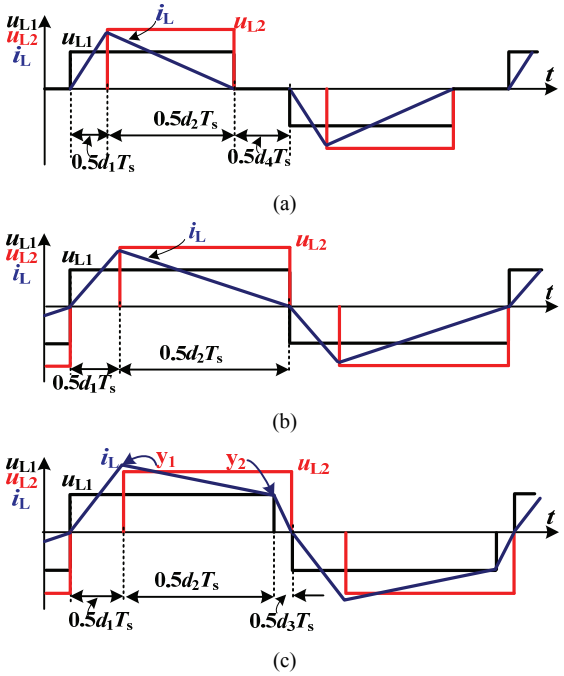

Fig. 5. Modulation strategy for the unified high-frequency bipolar boost principle. (a) DCM. (b) B-BCM. (c) BCM.

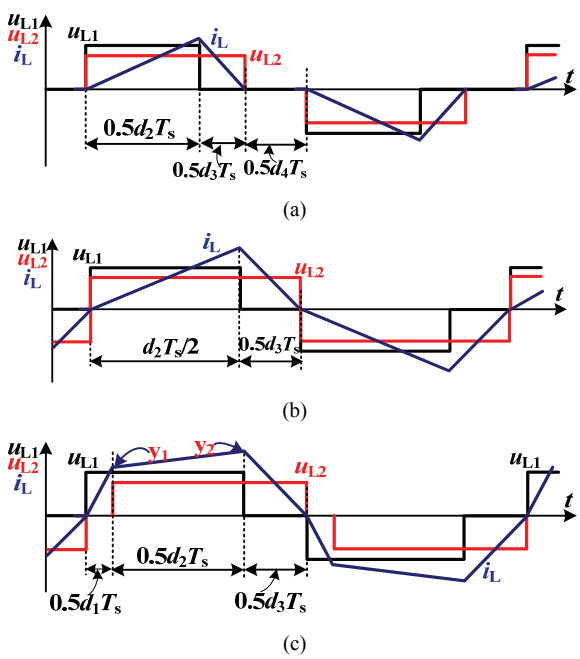

Fig. 6. Modulation strategy for the unified high-frequency bipolar buck principle. (a) DCM. (b) B-BCM. (c) BCM.

Fig. 6 and its boundary power is P_{B_buck}. The two boundary powers P_{B_boost} and P_{B_buck} can be obtained from the relationship in Fig. 5(b) and Fig. 6(b).

$$\begin{cases} P_{B\_boost} = \dfrac{(U_o - nU_{in})U_{in}^2 T_S}{4LU_o} \\ P_{B\_buck} = \dfrac{(nU_{in} - U_o)U_o^2 T_S}{4n^3 LU_{in}} \end{cases} \quad (3)$$

The characteristics of the negative power flow are symmetrical with those of the positive power flow. In the following section, only the condition of the positive power flow is discussed.

From Fig. 5 and Fig. 6, it can be seen that all of the modes obey the rule in Table II. However, not all of d_1-d_4 are more than 0. Thus, a simple and unified algorithm can be used to solve these four duty-ratios. Moreover, there is no circulating current in the converter, and all of the switches can achieve ZVS or ZCS in all occasions. Hence, the object presented in Section II can be satisfied.

IV. Algorithm to Solve Multiple Variables

In Fig. 5(c) and Fig. 6(c), y_1 and y_2 are the current values of i_L at the end of the first and second modes, respectively. Their expressions are independent of the size of nU_{in} and U_o. The operation conditions of the DCM and the B-BCM are also included in the operation condition of the BCM. For example, if d_1=0 and d_2+d_3<1, it is operated in the bipolar buck DCM. The other conditions can be summed up in Table III.

It should be noted that i_L is operated in the BCM or the DCM, which determines that i_L is equal to 0 at the beginning of the positive or negative half switching cycle. Therefore:

$$y_1 = \frac{U_{in} d_1 T_S}{2L} \tag{4}$$

$$y_2 = \frac{nU_{in} T_S d_1 + (nU_{in} - U_o) T_S d_2}{2nL} \tag{5}$$

The third duty ratio, d_3, can be achieved according to equilibrium of the current increasing and decreasing.

$$d_3 = \frac{nU_{in} d_1 + (nU_{in} - U_o) d_2}{U_o} \tag{6}$$

The part of i_L in modes 2 and 3 can be delivered to the filter capacitor in the HVS, while i_L in mode 1 cannot be delivered to the filter capacitor in the HVS. Hence, the following relationship can be achieved based on the fact that the output current I_o in the primary side is equal to the mean value of i_L in modes 2 and 3.

$$\begin{aligned} &d_2^2 (nU_{in} - U_o) + d_2 (2nd_1 U_{in} + nd_3 U_{in} - d_3 U_o) \\ &+ nd_1 d_3 U_{in} - 4n^2 L I_o / T_S = 0 \end{aligned} \tag{7}$$

The variable d_3 in (7) can be replaced by (6). Then:

$$\begin{aligned} &d_2^2 (nU_{in}(nU_{in} - U_o)) + d_2 (2n^2 U_{in}^2 d_1) \\ &+ n^2 U_{in}^2 d_1^2 - 4n^2 L U_o I_o / T_S = 0 \end{aligned} \tag{8}$$

Solving the solution of (8), it is possible to achieve:

$$d_2 = \frac{x_2 d_1 + \sqrt{x_3 d_1^2 + x_4}}{x_1} \tag{9}$$

$$d_3 = x_5 d_1 + x_6 d_2 \tag{10}$$

TABLE III
Relationship Between the Operation Condition and the Duty Ratios

	DCM	B-BCM	BCM
bipolar boost	d_3=0; d_1+d_2<1; $d_4=1-d_1-d_2$	d_1+d_2=1; d_3=0; d_4=0	$d_1+d_2+d_3$=1; d_4=0
bipolar buck	d_1=0; d_2+d_3<1; $d_4=1-d_2-d_3$	d_2+d_3=1; d_1=0; d_4=0	$d_1+d_2+d_3$=1; d_4=0

where:

$$x_1 = U_{in}(nU_{in} - U_o), \quad x_2 = -nU_{in}^2, \quad x_3 = nU_{in}^3 U_o,$$

$$x_4 = \frac{4nU_{in} U_o L I_o (nU_{in} - U_o)}{T_S}, \quad x_5 = \frac{nU_{in}}{U_o}, \quad x_6 = \frac{(nU_{in} - U_o)}{U_o}$$

According to Fig. 5 and Fig. 6, i_L can be divided into three parts in a half switching cycle, and only the parts in modes 2 and 3 can be delivered to the output filter capacitor. Hence, if (d_2+d_3) is bigger, i.e. the waveform of i_L is smooth, the current stress of the switches is smaller under the same output power. Setting $y= d_2+d_3$, the task of the algorithm is to deduce the proper value of d_1, d_2 and d_3 when y is at its maximum value. Substituting (9) and (10) into the expression of y yields:

$$y = x_5 d_1 + (1 + x_6) \frac{x_2 d_1 + \sqrt{x_3 d_1^2 + x_4}}{x_1} \tag{11}$$

Taking the derivative with respect to d_1 yields:

$$\frac{dy}{d(d_1)} = x_5 + \frac{x_2 (1 + x_6)}{x_1} + \frac{x_3 (1 + x_6) d_1}{x_1 \sqrt{x_3 d_1^2 + x_4}} = \frac{x_2}{x_1} + \frac{x_3 (1 + x_6) d_1}{x_1 \sqrt{x_3 d_1^2 + x_4}} \tag{12}$$

Setting (12) equal to 0, the value of d_1, which is denoted by d_{1y}, can be achieved when y is at its maximum value.

$$d_{1y} = \sqrt{\frac{x_4 x_2^2}{(x_3 + x_3 x_6)^2 - x_3 x_2^2}} \tag{13}$$

Solving the parameters d_1, d_2 and d_3 has three possibilities depending on the size of nU_{in} and U_o and the sum of d_1, d_2 and d_3.

A. $nU_{in} \geq U_o$

Under this condition, x_1 and x_3-x_6 are all more than zero, while x_2<0. Therefore, the quantity under the square root sign in (9) is automatically more than zero. If d_2 is guaranteed to be a positive value, it must satisfy (14).

$$d_{1x1}=0 \leq d_1 \leq \sqrt{\frac{x_4}{(x_2^2 - x_3)}} = d_{1z1} \tag{14}$$

After substituting the values of d_{1x1}, d_{1y} and d_{1z1} into (11), the value of d_1 can be selected as one of d_{1x1}, d_{1y} or d_{1z1}, which guarantees that the value of y is at its maximum.

B. $nU_{in} < U_o$

Under this condition, x_1, x_2, x_4 and x_6 are all less than zero, while x_3 and x_5 are more than zero. The quantity under the square root sign in (9) and the value of d_2 must be all more than

zero. Thus, it must satisfy the following expression.

$$d_{1x2}=\sqrt{\frac{-x_4}{x_3}} \le d_1 \le \sqrt{\frac{-x_4}{(x_3-x_2^2)}}=d_{1z2} \tag{15}$$

After substituting the values of d_{1x2}, d_{1y} and d_{1z2} into (11), the value of d_1 can be selected as one of d_{1x2}, d_{1y} or d_{1z2}, which guarantees that y is at its maximum value.

The values of d_2 and d_3 can be easily obtained from (9) and (10).

Another possible condition is $d_1+d_2+d_3>1$ which states that a variable-frequency is needed in the modulation. To realize constant -frequency control, the value of $d_1+d_2+d_3$ must be equal to 1, which is viewed as one of the known conditions.

C. $d_1+d_2+d_3=1$

First, d_3 can be determined according to this known condition.

$$d_3=1-d_1-d_2 \tag{16}$$

Under this condition, (8) is still correct and the d_3 in (16) can be substituted by (8). Then:

$$d_2=\frac{U_o-(nU_{in}+U_o)d_1}{nU_{in}} \tag{17}$$

If the d_2 in (17) is guaranteed to be a positive value:

$$d_1 \le \frac{U_o}{nU_{in}+U_o} \tag{18}$$

Eq. (8) is still correct and the d_2 in (17) can be substituted by (8). Then:

$$\begin{aligned}&(n^2U_{in}^2+nU_{in}|u_G|+U_o^2)d_1^2-\\&2U_o^2d_1+U_o^2-nU_{in}U_o^2+\frac{4n^3U_{in}Li^*}{T_S}=0\end{aligned} \tag{19}$$

The value of d_1 can be determined according to (18) and (19).

$$d_1=\frac{-b-\sqrt{b^2-4ac}}{2a} \tag{20}$$

where:

$$a=n^2U_{in}^2+nU_{in}U_o+U_o^2$$

$$b=-2U_o^2 \qquad c=U_o^2-nU_{in}U_o+\frac{4n^3U_{in}LI_o}{T_S}$$

The values of d_2 and d_3 can be achieved according to (16) and (17). The whole process for the calculation of d_1, d_2 and d_3 described above is shown in Fig. 7. It is noted that the load-current I_o is substituted by the reference current I_o*. The process in the flowchart shown in Fig. 7 is in accordance with the calculation process (4)-(20), which can be easily realized by a digital signal processor (DSP).

The switch driven signals can be obtained by a proper modulation strategy after achieving the values of d_1, d_2 and d_3. The control strategy for a DAB is shown in Fig. 8. It can be seen that the current sensor can be removed and that there is no feedback variable in the current inner-loop when compared

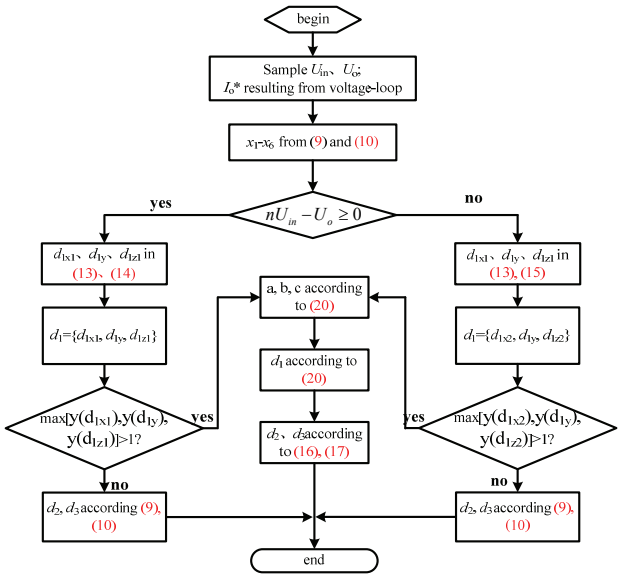

Fig. 7. Flowing chart for solving multi-variables.

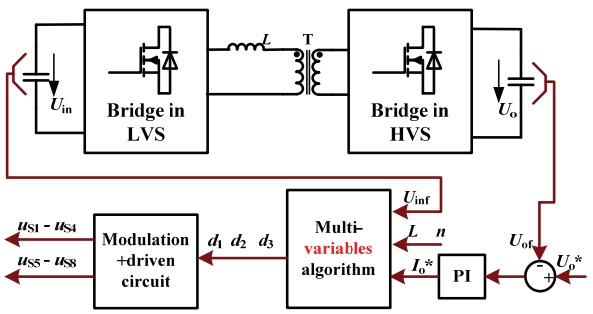

Fig. 8. Bipolar buck/boost control strategy for a DAB.

with the conventional method, which can greatly improve the dynamic performance.

Fig. 9 shows that the duty ratio curves vary with the output power and different input voltage when U_o=380V, L=6μH and n=380/49. The multi-duty-ratios have the following characteristics.

1. d_1 is always more than d_3 when $nU_{in}<U_o$ because the boost voltage is dominant in this time, and vice versa. In addition, d_1 is always less than d_3 when $nU_{in}>U_o$ because the buck voltage is dominant in this time. When $nU_{in}=U_o$, d_1 is always equal to d_3.
2. The sum of d_1, d_2 and d_3 becomes gradually larger with the output power increasing, and the DAB is operated in the BCM when $d_1+d_2+d_3=1$.
3. The DAB is operated in the BCM when $U_{in}=U_o/n$ and the boundary power in this time is zero. The boundary power gradually becomes larger when U_{in} is far from U_o/n. The lager the difference between U_{in} and U_o/n is, the smaller the operation range of the BCM becomes. The boundary power curve is shown in Fig. 10 according to (2) and (3).
4. Not all of the conditions have four modes. For example, the first mode does not exist when $d_1=0$ and the fourth mode does not exist when $d_1+d_2+d_3=1$.

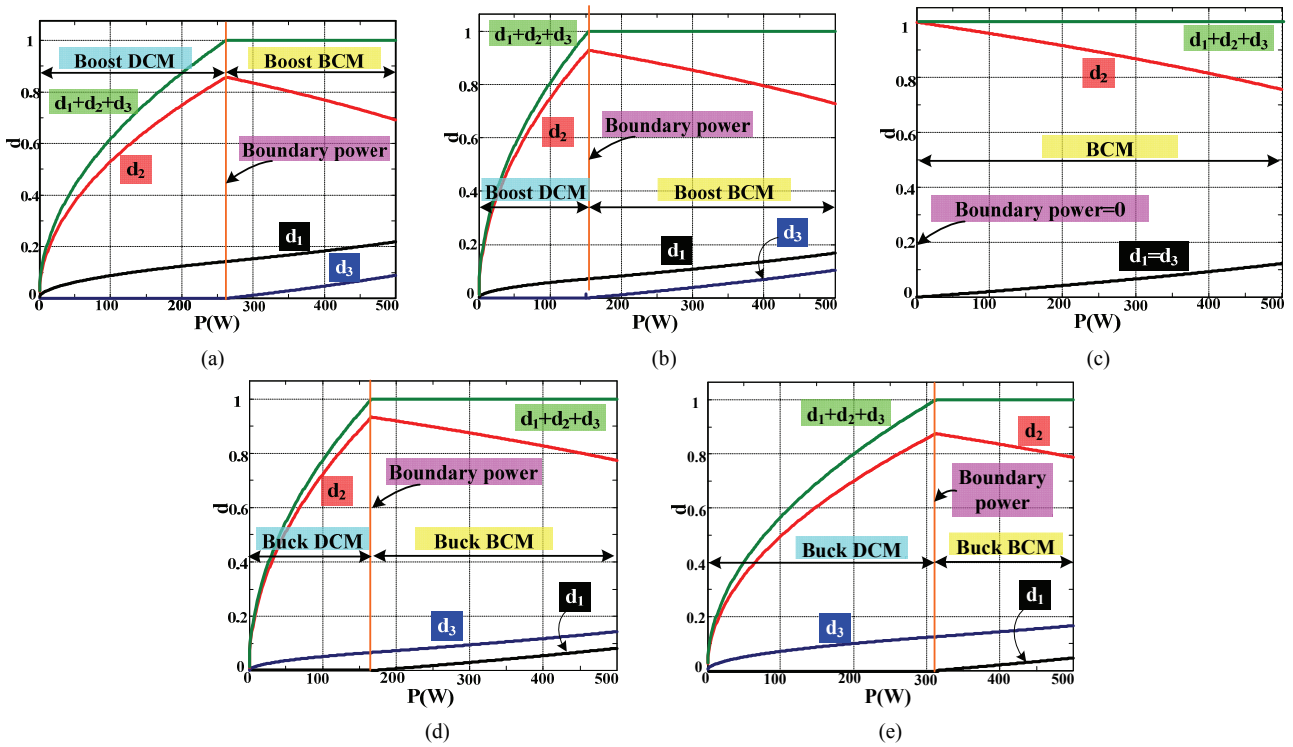

Fig. 9. Duty ratio curves varying with the output power. (a) U_{in}=42V. (b) U_{in}=45.5V. (c) U_{in}=49V. (d) U_{in}=52.5V. (e) U_{in}=56V.

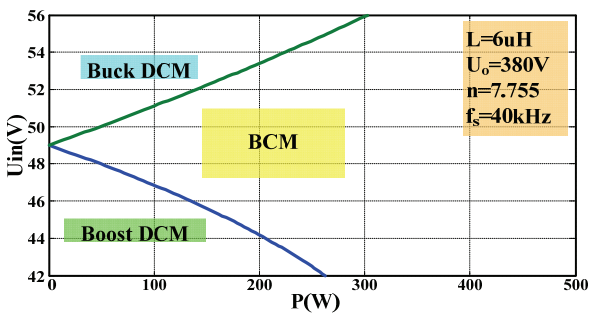

Fig. 10. Boundary power curve varying with the output power.

V. Parameters Design

Two parameters should be deliberatively designed in the main circuit of the DAB shown in Fig. 1. One is the transformer turns ratio n and the other is the inductance L. The current stress of the switch is at its minimum when the input voltage U_{in} is equal to the output voltage in the primary-side of the transformer (U_o/n). Considering the fluctuation range of U_{in}, n is set to U_o/U_{in_mid}, where U_{in_mid} is the mid-point value of the fluctuation range of U_{in}.

A typical application of a DAB is the charger and discharger for an accumulator in a DC micro-grid. The typical parameters are: U_{in} 42-56V, U_o 380V, switching frequency 40kHz, and rated power 500W.

U_{in_mid}, the mid-point value of the fluctuation range of U_{in}, is equal to 49V. Thus, the transformer turns ratio n can be determined by U_o/U_{in_mid} and its value is 7.755(380/49). There are two methods to design the inductance L in [12]. One method is that the value of L should be as small as possible to decrease the reactive power. The other method aims at expanding the range of ZVS, and the value of L should be as large as possible under the condition of guaranteeing the rated output power. These two methods have their advantages and disadvantages. In this paper, the value of L is designed for the minimum RMS value of i_L, which is proportional to the switches RMS current.

The subsection function of i_L in Fig. 5 and Fig. 6 can be achieved according to y_1 and y_2 in (4) and (5) in a half switching cycle. Thus, the RMS value of i_L can be obtained.

$$I_L = \sqrt{\frac{y_1^2(d_1+d_2)+y_2^2(d_2+d_3)+y_1y_2d_2}{3}} \tag{21}$$

The calculation of I_L needs to know the values of d_1, d_2 and d_3. However, they cannot be expressed by a continuous function. A simulation model for calculating d_1, d_2 and d_3 is built using MATLAB/Simulink. The achieved duty ratios are used to calculate I_L. The curves of I_L, varying with the input voltage, are shown in Fig. 11 with different output powers and different values of the inductance L. It can be seen that I_L is small with a bigger inductance (such as 10μH in the figure) under a light load. However, I_L increases quickly with a larger inductance when compared with a smaller inductance when the output power increases. The value of I_L is big and becomes violent with variations of the input voltage U_{in} under a smaller inductance (such as 2.5μH in the figure). Therefore, the principle for selecting the inductance is to avoid the two conditions mentioned above. The mediate values, such as 5μH

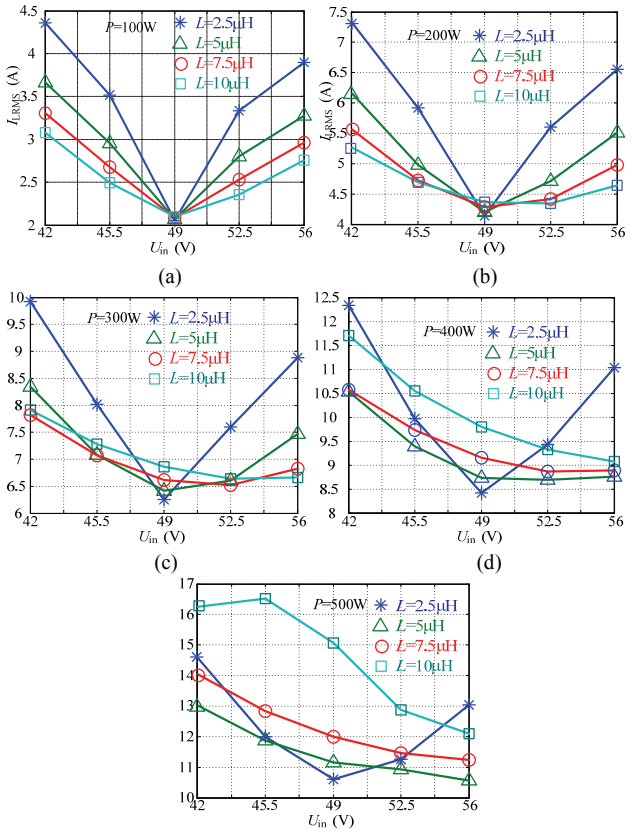

Fig. 11. I_L curves varying with U_{in} using different inductors. (a) P=100W. (b) P=200W. (c) P=300W. (d) P=400W. (e) P=500W.

and 7.5μH, are satisfied with the principle. On the one hand, I_L changes smoothly with a varying of the input voltage. On the other hand, I_L is at its optimized state from a light load to a full load. Considering the overall condition mentioned above, L=6μH is selected.

VI. Current Stress Comparison with the Closed Form Method

In [24], a closed form solution strategy has been proposed to achieve the optimized RMS value of i_L and the minimum conduction loss. Thus, the RMS value of i_L controlled by the proposed method in this paper is compared with the closed form solution strategy for determining the advantages and disadvantages of the proposed modulation strategy in this paper.

According to the strategy in [24], it is possible to obtain the transformer turns ratio n_1=7.755 and the optimized inductance L_1=12.86μH with the same input voltage, output voltage and output power. Fig. 12 shows an I_L value comparison between the closed form solution in [24] and the method proposed in this paper. The comparison results are as follows.

1. The I_L value controlled by the proposed method is a little more than that of the strategy in [24] under a light load, which can be seen from 100W curves.

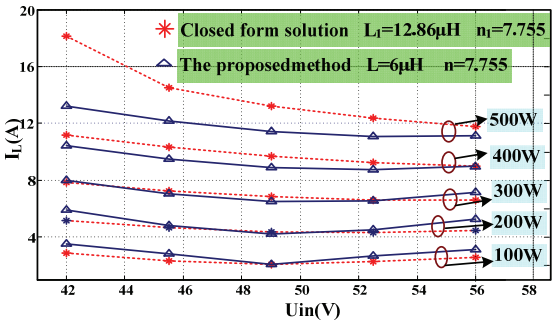

Fig. 12. I_L value comparison between the closed form solution and the method proposed in his paper.

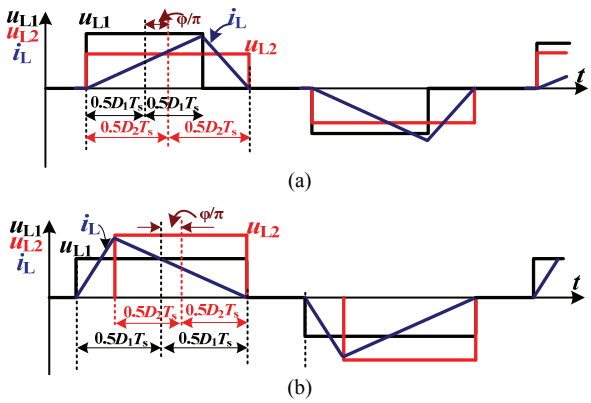

Fig. 13. Modulation strategy of TCM in [24] under a light load. (a) U_{in}>U_o/n. (b) U_{in}<U_o/n.

2. The I_L value controlled by the proposed method is approximately equal to that of the strategy in [24] when the output power is near 300W.
3. The I_L value controlled by the proposed method is significantly less than that of the strategy in [24] when the output power is greater than 300W.
4. The I_L value controlled by the proposed method is less than that of the strategy in [24] in the whole output range when U_{in}= U_o/n.

It can be seen that the method proposed in this paper has a larger current stress when compared with the strategy in [24] under a light load. However, it can be found that the modulation strategy in the proposed method under a light load is identical to that of the strategy in [24]. The larger current stress under a light load with the proposed strategy results from the small inductance of the buffering inductor. Fig. 13 shows waveforms from [24] using triangular current mode modulation (TCM). There are three parameters in the TCM: the primary-side bridge duty-ratio D_1, the secondary-side bridge duty-ratio D_2 and their phase-shift angle φ. Moreover, φ= D_1-D_2 when U_{in}< U_o/n, and φ= D_2-D_1 when U_{in}> U_o/n. Although the control parameters of the proposed method and the closed-form solution in [24] are different, the essentials of their operation are the same under a light load. The reason for a lager I_L under a light load of the proposed strategy is that it uses a smaller

TABLE IV
PARAMETERS FOR THE DAB PROTOTYPE

Components	Parameters
Input voltage U_{in}	42-56V
Output voltage U_o	380V
n	7.755
S1-S4	IRFB4110
S5-S8	C2M0080120D
P_{max}	500W
L	6μH

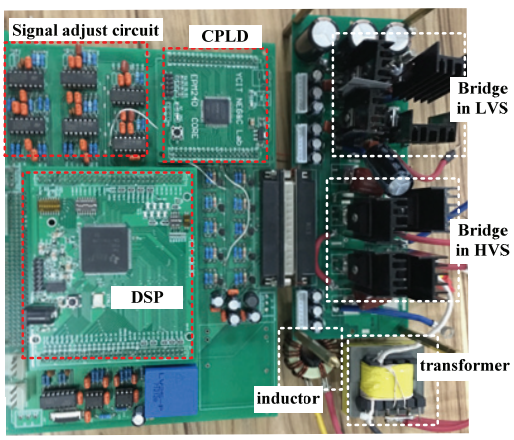

Fig. 14. Photo of the prototype.

inductance in the proposed method. The larger inductance can make the current waveform smooth when i_L is operated in the DCM, which leads to a smaller RMS value of i_L.

Therefore, the requirements in Section II, such as soft switching, no circulating current, low current stress and high efficiency are fulfilled.

VII. EXPERIMENTAL VERIFICATION

In order to verify the performance of the proposed control strategy, a 500W prototype is implemented. The circuit components and electric specifications are chosen as Table IV and a photo of the prototype is shown in Fig. 14.

Fig. 15(a)-(c) show waveforms under different input voltages when the output power is 300W. It can be seen that all three conditions are operated under the BCM, i.e. $d_1+d_2+d_3=1$, which guarantees a smaller current stress of the switches. However, the value of $(d_1+d_2+d_3)$ is less than 1 with a decrease of the output power. Fig. 15(d) shows the condition where the DAB is operated in the DCM when U_{in}=42V and P=100W. At this time, the DAB is at a voltage boost and d_3 is equal to zero.

Fig. 16 shows waveforms of a leading switch and a lagging switch in the LVS. Fig. 16(a) shows waveforms of the leading switch S1, which include its driven waveform u_{S1}, the voltage across the drain and source terminals u_{DS1}, and its through current i_{DS1}. There is almost no voltage spike in u_{DS1}. Fig. 16(b) and Fig. 16(c) are the turning on and turning off processes of

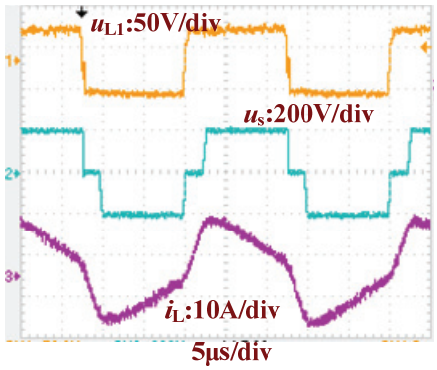

(a)

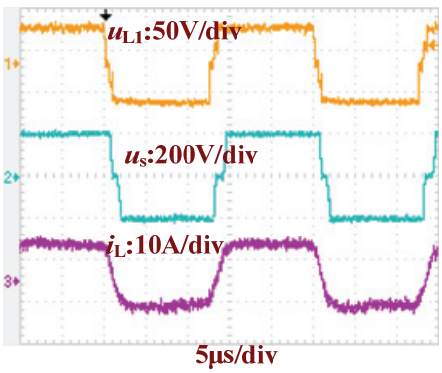

(b)

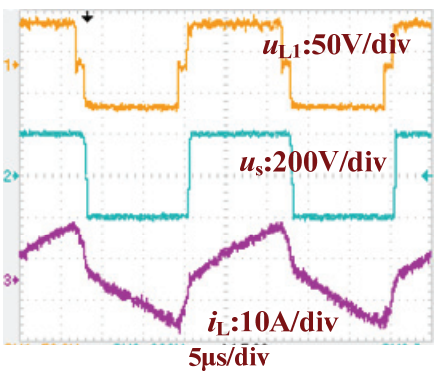

(c)

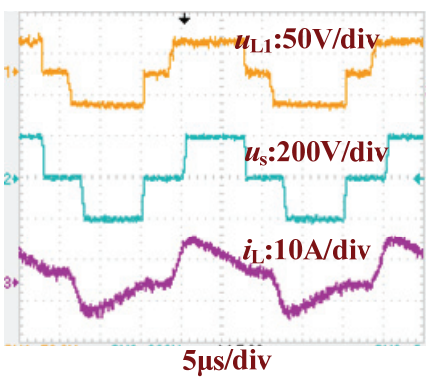

(d)

Fig. 15. Waveforms of a DAB with different input voltages and powers. (a) U_{in}=42V, P=300W. (b) U_{in}=49V, P=300W. (c) U_{in}=56V, P=300W. (d) U_{in}=42V, P=100W.

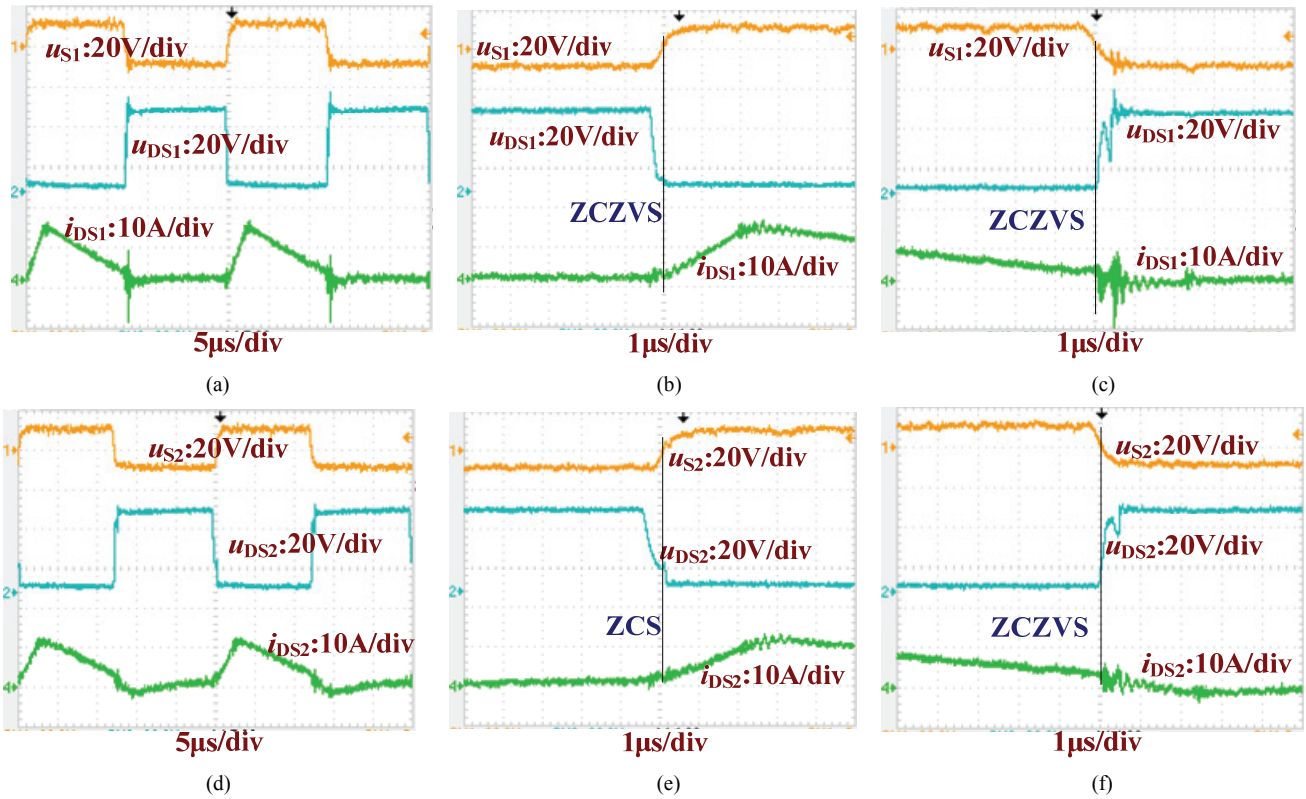

Fig. 16. Soft switching condition of switches in the LVS. (a) Waveforms of the leading switch S1. (b) Turn on process of S1. (c) Turn off process of S1. (d) Waveforms of the lagging switch S2. (e) Turn on process of S2. (f) Turn off process of S2.

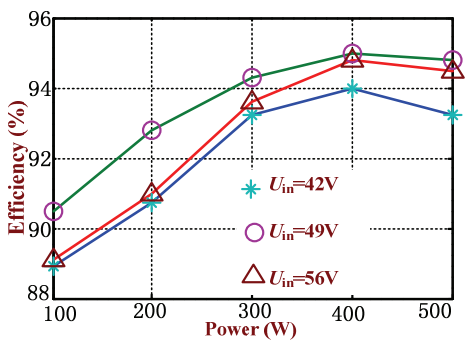

Fig. 17. Efficiency of a DAB under the control of the proposed strategy.

S1, respectively. Fig. 16(d) shows waveforms of the lagging switch S2, and Fig. 16(e) and Fig. 16(f) are the turning on and turning off processes of S2, respectively. The soft switching condition of S2 is same as that of the leading switch S1. It can be seen that the switches in the LVS can also obtain ZVZCS, regardless of the leading switch or the lagging switch.

Efficiency curves of the proposed control strategy for a DAB are shown in Fig. 17. It can be seen that the maximum efficiency is about 95%. The whole efficiency is at its highest when U_{in}=49V because the current stress is smallest under the same power.

The main loss of a DAB includes the conduction loss of the switches S1-S4 P_{con_S14}, the conduction loss of the switches S5-

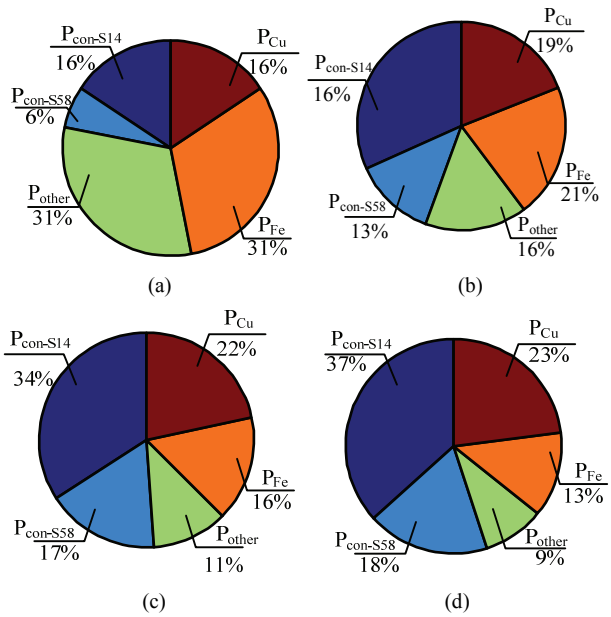

Fig. 18. Pie diagrams of the loss breakdown of a DAB controlled by the proposed strategy when the input voltage is U_{in}=42 V. (a) P= 125W. (b) P = 250W. (c) P = 375W. (d) P = 500W.

S8 P_{con_S58}, the core loss and copper loss of the buffering inductor and transformer P_{Fe}, P_{Cu}. Some other loss P_{other}, such as the losses in the driving circuit, auxiliary power supply, DSP and other analog chips, occupies a small percentage of the total

loss. Fig. 18 shows the loss percentage of the different kinds of losses mentioned above. P_{Fe} and P_{Cu} are the main loss under a light load. Under a heavy load, the conduction loss of the switches are the main loss in a DAB.

VIII. CONCLUSION

A control strategy for a DAB based on the high-frequency bipolar buck-boost principle is proposed in this paper. This strategy is derived from the classical DC/DC buck and boost converter operation principle. The proposed strategy guarantees that the inductor current is operated in the DCM or the BCM which leads to ZVS or ZCS of the switches, and high efficiency. An algorithm for solving the multi-variables is proposed and the specific flow is given. The calculation flow is simple and can be easily realized by a DSP. According to the solution of the multi-duty-ratios, the RMS value of i_L can be achieved, which is used to determine the parameters of the turns ratio and inductance. Experimental results verify that the proposed method has high performance.

REFERENCES

[1] R. T. Naayagi, A. J. Forsyth, and R. Shuttleworth, "High-power bidirectional DC–DC converter for aerospace applications," *IEEE Trans. Pow. Electron*., Vol. 27, No. 11, pp. 4366-4379, Nov. 2012.

[2] S. Choi, Y. Kim, I. Lee, and J. Lee, "Isolated PFC converter based on an ADAB structure with harmonic modulation for EV chargers," *J. Power Electron.*, Vol. 18, No. 2, pp. 383-394, Mar. 2018.

[3] B. Zhao, Q. Song, and W. Liu, "A practical solution of high-frequency-link bidirectional solid-state transformer based on advanced components in hybrid microgrid," *IEEE Trans. Ind. Electron*., Vol. 62, No. 7, pp. 4587-4597, Jul. 2015.

[4] H. Ardi, R. R. Ahrabi, and S. N. Ravadanegh, "Non-isolated bidirectional DC-DC converter analysis and implementation," *IET Power Electron.*, Vol. 7, No. 12, pp. 3033-3044, Dec. 2013.

[5] J. Kan, S. Xie, Y. Tang, and Y. Wu, "Voltage-fed dual Active bridge bidirectional DC/DC converter with an immittance network," *IEEE Trans. Power Electron.*, Vol. 29, No. 7, pp. 3582-3590, Jul. 2014.

[6] X. Pan and A. K. Rathore, "Current-fed soft-switching push–pull front-end converter-based bidirectional inverter for residential photovoltaic power system," *IEEE Trans. Power Electron.*, Vol. 29, No. 11, pp. 6041-6051, Nov. 2014.

[7] L. Jiang, Y. Sun, M. Su, H. Wang, and H. Dan, "Optimized operation of dual-active-bridge DC-DC converters in the soft-switching area with triple-phase-shift control at light loads," *J. Power Electron.*, Vol. 18, No. 1, pp. 45-55, Jan. 2018.

[8] S. Y. Tseng, C. T. Hsieh, and C. M. Yang, "Interleaved flyback converter with turn-on/off for poultry stunning applications," in *Proc. IEEE APEC*, pp. 1999-2005, 2008.

[9] F. Zhang and Y. Yan, "Novel forward–flyback hybrid bidirectional DC–DC converter," *IEEE Trans. Ind. Electron.*, Vol. 56, No. 5, pp. 1578-1584, May 2009.

[10] F. Z. Peng, L. Hui, and S. G. Jia, "A new ZVS bidirectional DC–DC converter for fuel cell and battery application," *IEEE Trans. Power Electron.*, Vol. 19, No. 1, pp. 54-65, Jan. 2004.

[11] G. G. Oggier and M. Ordonez, "High efficiency DAB converter using switching sequences and burst-mode," *IEEE Trans. Pow. Electron.*, Vol. 31, No. 3, pp. 2069-2082, Mar. 2016.

[12] A. Rodr´ıguez, A. V´azquez, and D. G. Lamar, "Different purpose design strategies and techniques to improve the performance of a dual active bridge with phase-shift control," *IEEE Trans. Pow. Electron.*, Vol. 30, No. 2, pp. 790-804, Feb. 2015.

[13] W. Lee, H. Choi, Y. Cho, M. Ryu, and J. Jung, "Design methodology of a three-phase dual active bridge converter for low voltage direct current applications," *J. Power Electron.*, Vol. 18, No. 2, pp. 482-491, Mar. 2018.

[14] H. Bai and C. Mi "Eliminate reactive power and increase system efficiency of isolated bidirectional dual-active-bridge DC–DC converters using novel dual-phase-shift control," *IEEE Trans. Pow. Electron.*, Vol. 23, No. 6, pp. 2905-2914, Jun. 2008.

[15] B. Zhao, Q. Yu, and W. Sun, "Extended-phase-shift control of isolated bidirectional DC–DC converter for power distribution in microgrid," *IEEE Trans. Pow. Electron.*, Vol. 27, No. 11, pp. 4667-4680, Nov. 2012.

[16] B. Zhao, Q. Song, and W. Liu, "Efficiency characterization and optimization of isolated bidirectional DC–DC converter based on dual-phase-shift control for DC distribution application," *IEEE Trans. Power Electron.*, Vol. 28, No. 4, pp. 1711-1727, Apr. 2013.

[17] Z. Zhang, Y. Cai, and Y. Zhang, "A distributed architecture based on micro-bank modules with self-reconfiguration control to improve the energy efficiency in the battery energy storage system," *IEEE Trans. Power Electron.*, Vol. 31, No. 1, pp. 304-317, Jan. 2016.

[18] F. Krismer and J. W. Kolar, "Efficiency-optimized high-current dual active bridge converter for automotive applications," *IEEE Trans. Power Electron.*, Vol. 27, No. 7, pp. 2745-2760, Jul. 2012.

[19] G. D. Demetriades and H. P. Nee, "Dynamic modeling of the Dual-Active Bridge topology for high-power applications," in *Proc. IEEE APEC*, pp. 15-19, 2008.

[20] T. Zhao, G. Wang, and S. Bhattacharya, "Voltage and power balance control for a cascaded H-bridge converter-based solid-state transformer," *IEEE Trans. Power Electron*, Vol. 8, No. 4, pp. 1523-1532, Apr. 2013.

[21] P. Cortes, M. P. Kazmierkowski, and R. M. Kennel, "Predictive control in power electronics and drives," *IEEE Trans. Ind. Electron.*, Vol. 55, No. 12, pp. 4312-4324, Dec. 2008.

[22] J. Kan, Y. Wu, Y. Tang, B. Zhang, and Z. Zhang, "Dual active full-bridge bidirectional converter for V2G charger based on high-frequency AC buck-boost control strategy," in *Proc. IEEE ITEC*, pp. 46-50, 2016.

[23] T. Hirose, M. Takasaki, and Y. Ishizuka, "A power efficiency improvement technique for a bidirectional dual active bridge dc-dc converter at light load," *IEEE Trans. Ind. Appl.*, Vol. 50, No. 6, pp. 4047-4055, Nov./Dec. 2014.

[24] F. Krismer and J. W. Kolar, "Closed form solution for minimum conduction loss modulation of DAB converters," *IEEE Trans. Power Electron.*, Vol. 27, No. 1, pp. 174-188,

Jan. 2012.
[25] H. Zhou and A. M. Khambadkone, "Hybrid modulation for dual-active bridge bidirectional converter with extended power range for ultracapacitor application," *IEEE Trans. Ind. Appl.*, Vol. 45, No. 4, pp. 1434-1442, Apr. 2009.
[26] F. J. Wu, F. Feng, and H. B. Goay, "Cooperative triple-phase-shift control for isolated DAB DC-DC converter to improve current characteristics," *IEEE Trans. Ind. Electron.*, Early Access, 2018.
[27] G. G. Oggier, G. O. GarcÍa, and A. R. Oliva ,"Switching control strategy to minimize dual active bridge converter losses," *IEEE Trans. Power Electron.*, Vol. 24, No. 7, pp. 1826-1838, Jul. 2009.

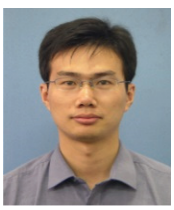

Jia-rong Kan was born in Jiangsu, China, in 1979. He received his M.S. degree in Electrical Engineering from the Nanjing University of Aeronautics and Astronautics (NUAA), Nanjing, China, in 2007. He joined the School of Electrical Engineering, Yancheng Institute of Technology, Yancheng, China, in 2007, where he is presently working as an Associate Professor. He is the holder of five patents and is the author or coauthor of more than 40 technical papers. His current research interests include power electronics in renewable energy generation.

Yao-dong Yang was born in Hebei Province, China. He received his B.S. degree in Electrical Engineering from the Hebei University of Technology, Tianjin, China, in 2017, where he is presently studying high frequency power electronics as a graduate student. His current research interests include power electronics and control, which include high frequency power conversions and specific harmonic elimination.

Yu Tang received his B.S. and Ph.D. degrees in Electrical Engineering from the Nanjing University of Aeronautics and Astronautics (NUAA), Nanjing, China, in 2003 and 2008, respectively. He joined the Department of Electrical Engineering, NUAA, in 2008, where he is presently working as an Associate Professor. He holds two Chinese patents and has published more than 50 papers in journals and conference proceedings. His current research interests include power electronics in renewable energy generation.

Dong-chun Wu was born in Jiangsu, China, in 1975. He received his M.S. degree in Material Processing Engineering from Hohai University, Nanjing, China, in 2007. After graduating, he joined the School of Electrical Engineering, Yancheng Institute of Technology, Yancheng, China, where he is presently working as an Associate Professor. He is the author or coauthor of more than 20 technical papers. His current research interests include power electronics in renewable energy generation and computer control technology.

Yun-ya Wu was born in Jiangsu, China, in 1979. She received her M.S. degree in Computer Technology from the Nanjing University of Science and Technology, Nanjing, China, in 2010. She joined the School of Electrical Engineering, Yancheng Institute of Technology, Yancheng, China, in 2001, where she is presently working as a Lecturer. Her current research interests include control strategies for the grid-connected inverters in microgrids.

Jiang Wu was born in Shandong, China. He received his B.S. degree from Shandong University, Jinan, China, in 2013. From 2013 to 2017, he was a Junior Electrical Engineer for the State Grid of China. From 2017 to 2018, he worked as a Senior Electrical Engineer for the State Grid of China. His current research interests include power electronics and control, which include the fault diagnosis of electrical machines, new energy generation, control technologies, and relay protection technology of power systems.